

RESEARCH PAPER

Antifungal Efficacy of Chitosan-Modified Zinc Oxide Nanoparticles on Tube Sedge Products

Pachara Pholnak¹, Jidapa Khongbun², Kullanan Suksom², Monthon Lertworapreecha³, Sumetha Suwanboon⁴, and Chitnarong Sirisathitkul^{5*}

¹ Department of Physics, Faculty of Science, Thaksin University, Phatthalung, 93210 Thailand

² Paphayomphittayakom School, SciUS-TSU, Phatthalung, 93210 Thailand

³ Department of Biology, Faculty of Science, Thaksin University, Phatthalung, 93210 Thailand

⁴ Department of Materials Science and Technology, Faculty of Science, Prince of Songkla University, Songkhla 90112, Thailand

⁵ Division of Physics, School of Science, Walailak University, Nakhon Si Thammarat 80160, Thailand

ARTICLE INFO

Article History:

Received 03 January 2020

Accepted 11 March 2020

Published 01 April 2020

Keywords:

Basketry

Chitosan

Fungicide

Tube sedge

ZnO

ABSTRACT

The antifungal properties of ZnO were implemented in the real handicraft and showed promising results for the value addition of local products by sun-screen and fungi protections. The inhibition of *Aspergillus* sp. growth on tube sedge basketry by zinc oxide (ZnO) was demonstrated. ZnO nanoparticles synthesized with chitosan capping agents were analyzed by X-ray diffractometry (XRD), Fourier transform infrared (FTIR) spectrophotometry and thermogravimetric analysis (TGA). The crystallite size consistent with electron microscope images and surface area of ZnO were dependent on the amounts of chitosan. ZnO exhibited a large ultraviolet (UV) absorbance in an entire 200-400 nm range when large crystallites agglomerated into bulky aggregates. In the case of small amounts of chitosan used, small crystallites tending to agglomerate in close contacts enhanced antifungal activity on pieces of tube sedge basketry. The fungi inhibition by this chitosan-modified ZnO was attributed to the stress response in fungal hyphae and generation of hydrogen peroxide.

How to cite this article

Pholnak P, Khongbun J, Suksom K, Lertworapreecha M, Suwanboon S, Sirisathitkul C. Antifungal Efficacy of Chitosan-Modified Zinc Oxide Nanoparticles on Tube Sedge Products. *J Nanostruct*, 2020; 10(2):424-433. DOI: 10.22052/JNS.2020.02.020

INTRODUCTION

Zinc oxide (ZnO), an n-type direct band gap semiconductor, has been renowned for its applications in industry. Currently, more eco-friendly routes are developed to synthesize ZnO in forms of nanostructures [1-4]. Nanostructured ZnO exhibits multifunctionality based on its electric, optical, photocatalytic as well as antimicrobial properties. Direct contacts of ZnO on bacteria cells release of Zn²⁺ and reactive oxidation species (ROS) which are detriment to bacterial growth. For fungi, the exposure to ZnO nanoparticles

deforms the surface of fungal hyphae with increased nucleic acids and carbohydrates through the stress response in fungal hyphae [5]. Hydrogen peroxide generated from ZnO is also a major contributor of antifungal activity [6]. The rupture and the damage of the cell membrane reduce the fungal enzymatic activity and lead to cell deaths [7-10]. A high surface-to-volume ratio of ZnO nanoparticles then enhances antimicrobial activity compared to the bulk form. Lalithambika demonstrated that antibacterial efficiency of ZnO nanopowder was higher than that of NiO

* Corresponding Author Email: chitnarong.siri@gmail.com



This work is licensed under the Creative Commons Attribution 4.0 International License.

To view a copy of this license, visit <http://creativecommons.org/licenses/by/4.0/>.

counterpart [2]. The antimicrobial activity was successfully enhanced by doping ZnO with Ag [11], Co [12], Ni [13]. The doping of ZnO by either Co or Ni also led to dilute magnetic semiconductors. To increase antibacterial activity with the surface-to-volume ratio, the size of ZnO was regulated by capping agents such as polyethylene glycol [14] and chitosan [15]. Furthermore, a large variety of nanocomposites with antimicrobial activity were obtained by incorporating ZnO into other functional materials, e.g. polyaniline [16], CuO [3], rare-earth elements [17]. By virtue of these doping, surface modification and composites, the antimicrobial properties were enhanced by synergistic effects.

The antimicrobial agents from ZnO, doped-ZnO and ZnO nanocomposites are majorly exploited in nanomedicine and medical uses. Besides, these materials can be useful for food and handicraft products which are susceptible to microbial growths. Jamdagni and co-workers used ZnO in conjunction with common agricultural fungicide [8]. Such applications greatly benefit the community aiming to reduce the yield loss and health risk as well as to add the value of local products. This work emphasizes on the fungi inhibition on tube sedge (*Lepironia articulata* (Retz.) Domin) basketry which are used and sold by locals in several countries including the southern region of Thailand. The values of local handicrafts can be added by the ZnO coating for sun-screen and fungi protections.

MATERIALS AND METHODS

ZnO nanosuspensions were synthesized

from zinc acetate dihydrate ($\text{Zn}(\text{CH}_3\text{COO})_2 \cdot 2\text{H}_2\text{O}$; Ajax Finechem, 99.5%) and sodium hydroxide (NaOH; Merck, 99%) with chitosan as a capping agent. $\text{Zn}(\text{CH}_3\text{COO})_2 \cdot 2\text{H}_2\text{O}$ of 1.0975 g, 2.195 g, and 4.390 g was separately dissolved in 100 mL of distilled water to obtain the concentration of 0.05 M, 0.1 M, and 0.2 M whereas the chitosan (low MW-4000) of 1.25 g and 2.5 g chitosan (low MW-4000) was dissolved in 2% acetic acid. With varying concentrations shown by Table 1, both solutions were then mixed with 0.2 M NaOH solutions, giving rise to 6 samples referred to as C1-C6 in Table 1. All nanosuspensions were continuously stirred for 15 h. The pH was adjusted to 7 by NaOH solutions and the stirring was continued for another 4 h. The nanosuspensions were then sonicated for 4 h to enhance ZnO dispersion in nanosuspensions.

To characterize ZnO nanoparticles, nanosuspensions were centrifuged and the precipitates were filtered. The nanoparticles were repeatedly washed by ethanol and then dried at 60 °C for 15 h. Morphology of each sample were obtained from the scanning electron microscope (SEM, FEI Quanta 450 PEG) and transmission electron microscope (TEM, Tecnai G² 20) whereas optical properties were characterized by the UV-Vis spectrophotometer (Shimadzu UV-2450). Surface area and porosity were analyzed by the static volumetric nitrogen gas adsorption method (Micromerit ASAP 2460) according to Brunauer-Emmett-Teller (BET) theory.

The structure was characterized by the simultaneous thermal analyzer (Perkin Elmer, STA8000), Fourier transform infrared spectrophotometer (FTIR, Agilent Cary 630) and

Table 1. List of reagents used in the synthesis of ZnO nanosuspension. Crystallite sizes calculated from XRD peak widths of samples C1-C6 are also shown.

Sample Code	Concentration of reagents (M)		Mass (g)		Crystallite size (nm)	BET Surface Area (m ² /g)
	Zn(CH ₃ COO) ₂ · 2H ₂ O	NaOH	Zn(CH ₃ COO) ₂ · 2H ₂ O	Chitosan		
C1	0.05	0.2	1.098	1.25	48.5	1.87
C2	0.10	0.2	2.195	2.5	56.5	4.69
C3	0.20	0.2	4.390	1.25	38.8	1.82
C4	0.05	0.2	1.098	2.5	28.2	6.67
C5	0.10	0.2	2.195	1.25	28.2	1.24
C6	0.20	0.2	4.390	2.5	21.1	3.64

X-ray diffractometer (XRD, Philips X' Pert MPD). The average crystallite sizes of the particles (D) were calculated by using Debye-Scherrer equation:

$$D = \frac{0.9\lambda}{\beta \cos\theta} \quad (1)$$

where λ is the X-ray wavelength (1.54 Å). θ is the diffraction angle and β is the full width at half maximum of the major XRD peak.

To test antifungal efficacy using the zone of inhibition method, the suspension of the *Aspergillus* sp. was adjusted to approximately 10^6 conidia spore/mL by 0.85% normal saline and spread on potato dextrose agar (PDA) (Himedia, India). The nanosuspension was also sprayed on 1 inch² pieces of tube sedge basketry from local market. Before the fungi application, the tube sedge samples were heated at 60 °C for 4 h and coated with ZnO nanosuspension. Two other samples, one lacquer coating and a control without any coating, were also prepared for the comparison. The Preti dishes containing PDA and samples were incubated at room temperature. The growth of pathogenic fungi was monitored by taking photographs of the tube sedge pieces after 1, 10, 20 days of inoculation.

RESULTS AND DISCUSSION

TGA and DTG

As the temperature is raised up to 1000 °C in Fig. 1, the thermogravimetric analysis (TGA) curve exhibits the reductions in weight with changing slopes. Corresponding to the derivative thermogravimetry (DTG) curve, the different slopes indicate the occurrence of different processes. The drastic weight losses below 100 °C [18] and over 200 °C [3] are respectively due to the dehydration and the thermal decomposition of chitosan. The next weight loss is gradual in an extended range from 350 to 750 °C, covering both combustion of organic residuals and crystallization of nanostructured ZnO [19]. Around 760 °C, the remaining weight is only 35%.

FTIR

The characteristic vibration of each bonding can be detected by FTIR spectroscopy and the spectra of chitosan-modified ZnO are compared with the ZnO and chitosan standards in Fig. 2. For every spectrum, a broad peak centered around 3295 cm⁻¹ corresponds to the O-H vibration of adsorbed water molecules [1-3, 12, 13, 17]. This range also covers the vibration of amino group of chitosan [15]. The much smaller peaks at 2867 cm⁻¹

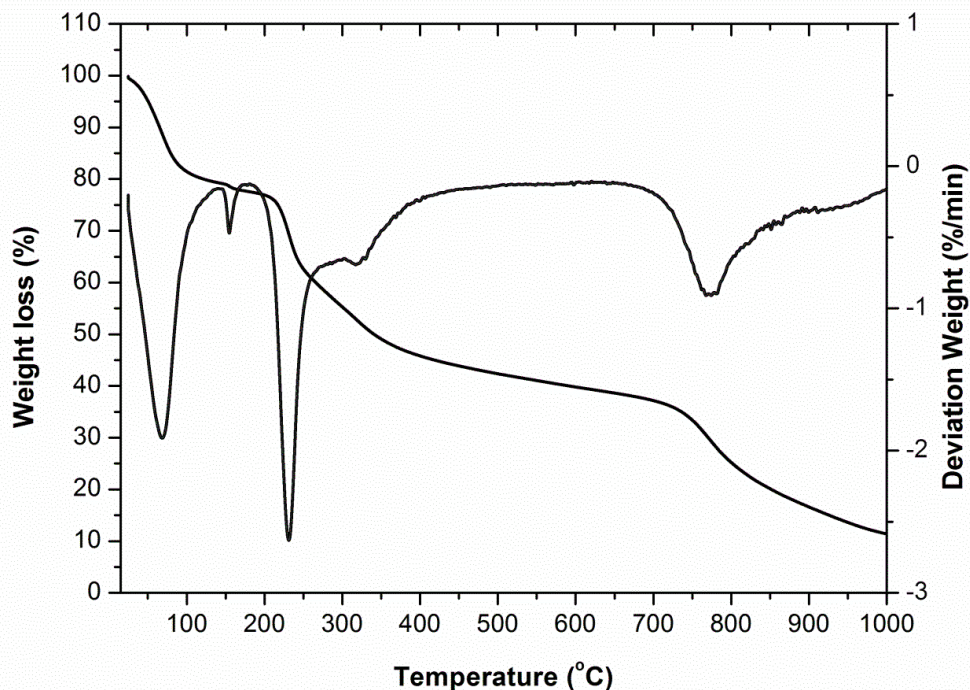


Fig. 1. TGA and DTG curves of chitosan-modified ZnO nanoparticles.

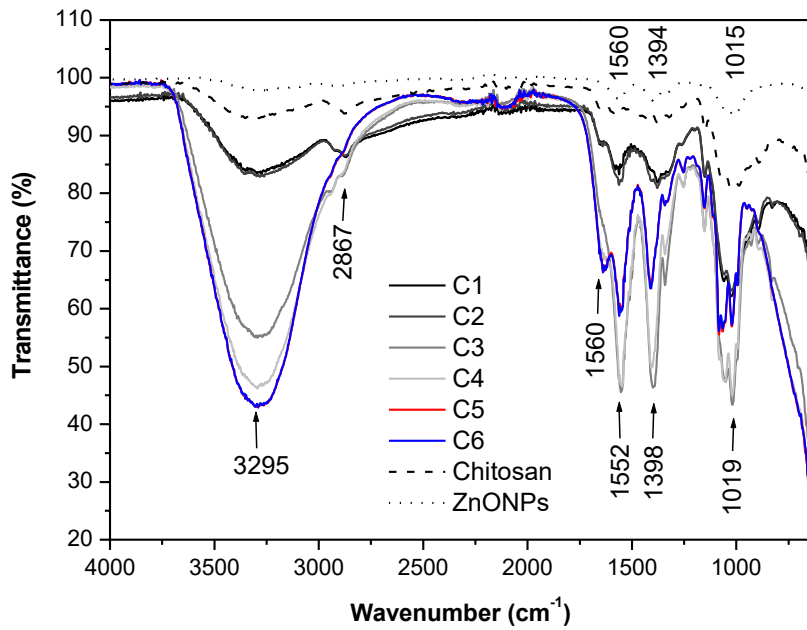


Fig. 2. FTIR spectra of chitosan-modified ZnO nanoparticles.

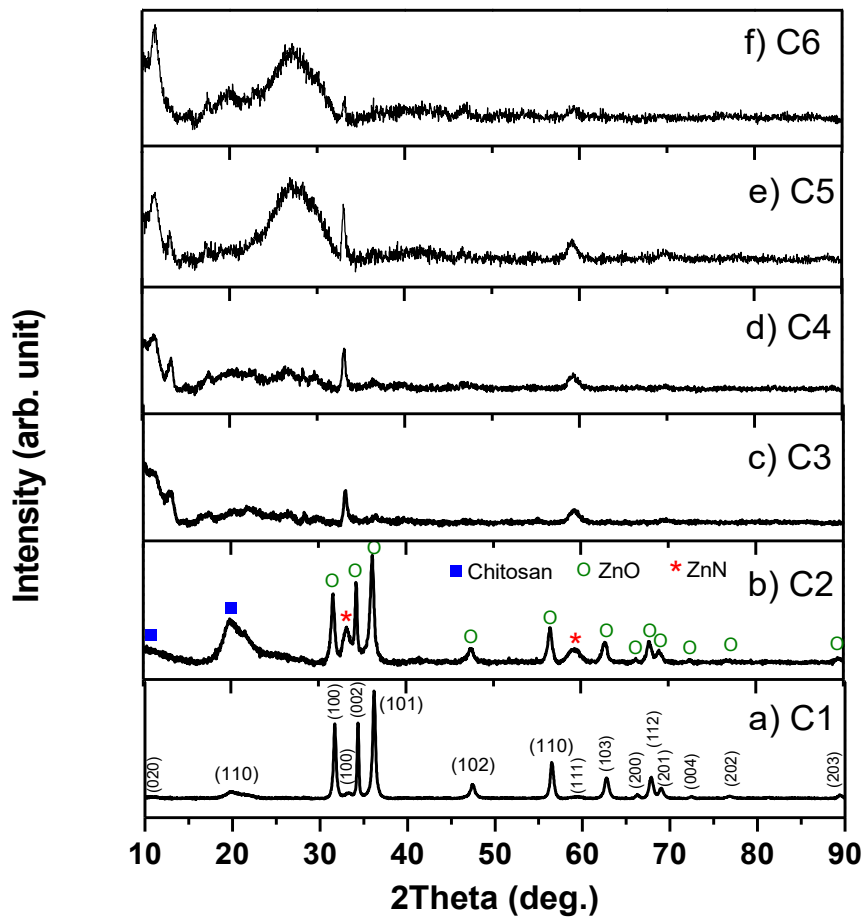


Fig. 3. XRD patterns of chitosan-modified ZnO nanoparticles.

are attributed to the -CH symmetric stretching [3, 13, 15]. Whereas the peak at 2350 cm^{-1} due to the absorption of atmospheric CO_2 on the metallic radicals is not clearly observed, chitosan and chitosan-rich samples have small but broad peaks at slightly lower wavenumbers [1, 13]. The peak at 1560 cm^{-1} is attributed to chitosan. Between 1000 cm^{-1} and 1500 cm^{-1} , there are a few sharp peaks corresponding to -NH, -CH, -NH,C=O and other residual free charges from impurities in the products [1, 2, 17]. The absorption peak around $470\text{-}530\text{ cm}^{-1}$ from the Zn-O stretching mode of vibration in ZnO structure is exclusively observed in ZnO sample [1-3, 12, 15-17]. Overall, the addition of chitosan in the ZnO synthesis largely

affects the intensity in IR absorption. Whereas all characteristic ZnO peaks appear at identical positions, the peak intensity is decreased with increasing chitosan.

XRD and microscope images

The phase identification by XRD is consistent with the characteristic vibration in FTIR spectra. XRD patterns in Fig. 3 exhibit peaks at 31.69° , 34.34° , 36.19° , 47.38° , 56.47° , 62.75° , 66.27° , 67.84° , 68.97° , and 72.37° by the diffraction respectively from (100), (002), (101), (102), (110), (103), (200), (112), (201), and (004) planes of the single phase ZnO with the hexagonal wurtzite structure (JCPDS card No.36-1451) [2, 3, 14, 17].

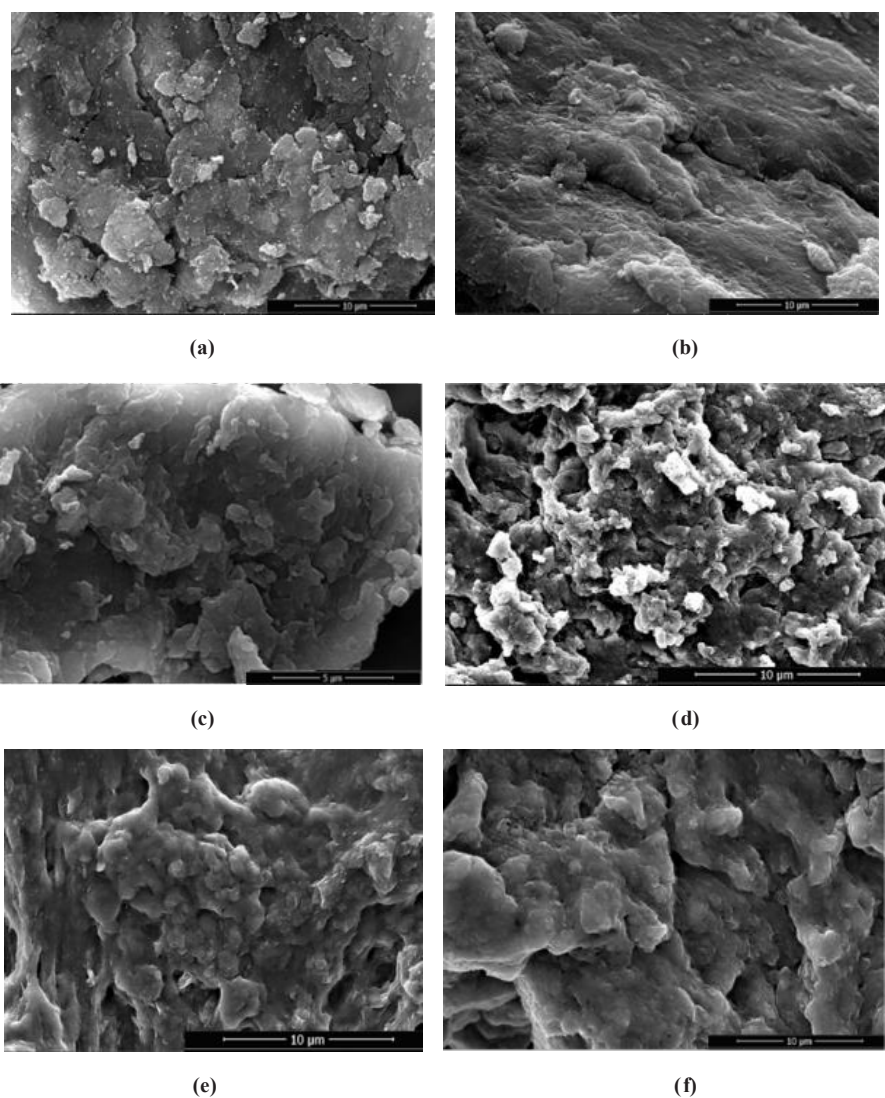


Fig. 4. SEM micrographs of chitosan-modified ZnO nanoparticles; samples (a) C1, (b) C2, (c) C3, (d) C4, (e) C5 and (f) C6.

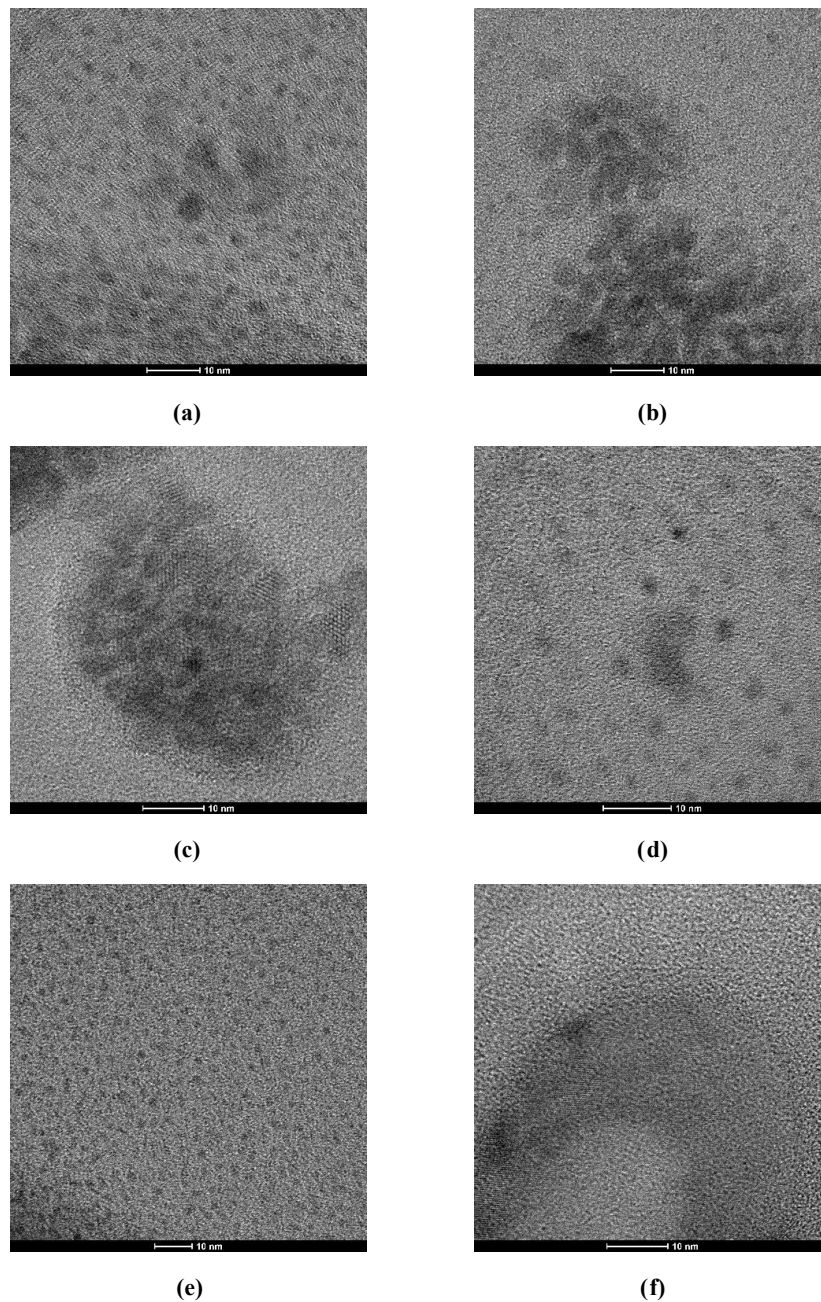


Fig. 5. TEM images of chitosan-modified ZnO nanoparticles; samples (a) C1, (b) C2, (c) C3, (d) C4, (e) C5 and (f) C6.

In addition to the characteristic ZnO peaks, broad peaks below 30° are assigned to the chitosan. With increasing $\text{Zn}(\text{CH}_3\text{COO})_2 \cdot 2\text{H}_2\text{O}$ in the synthesis, the peaks of samples C5 and C6 are shifted to a higher angle and grow at the expense of ZnO peaks. This evolution of XRD pattern signifies the encapsulation ZnO by chitosan. On the other hand, the lattice parameters of ZnO remains rather

constant as diffraction peaks from ZnO are at the same positions.

The crystallite sizes evaluated from the major ZnO peak width are shown in Table 1. In a range from 14-54 nm comparable to the literature [2, 3, 8, 14], smaller sizes are obtained in the case of samples C5 and C6 due to the encapsulation of ZnO by chitosan. Interestingly, the crystallite








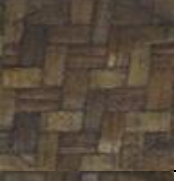











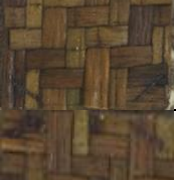

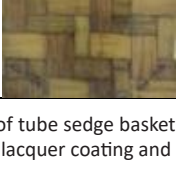


Tube Sedge Coating	Day 1	Day 10	Day 20
Control (without coating)			
Coated by lacquer			
Coated by ZnO sample C1			
Coated by ZnO sample C2			
Coated by ZnO sample C3			
Coated by ZnO sample C4			
Coated by ZnO sample C5			
Coated by ZnO sample C6			

Fig. 6. Comparison of pieces of tube sedge basketry coated by chitosan-modified ZnO nanoparticles with those of lacquer coating and no coating after 1, 10 and 20 days.

size can be related to the morphology shown by SEM images in Fig. 4 and the samples can then be

divided into 2 groups. In the first group of samples C1-C3 with the crystallite size of 38.8-56.5 nm, ZnO

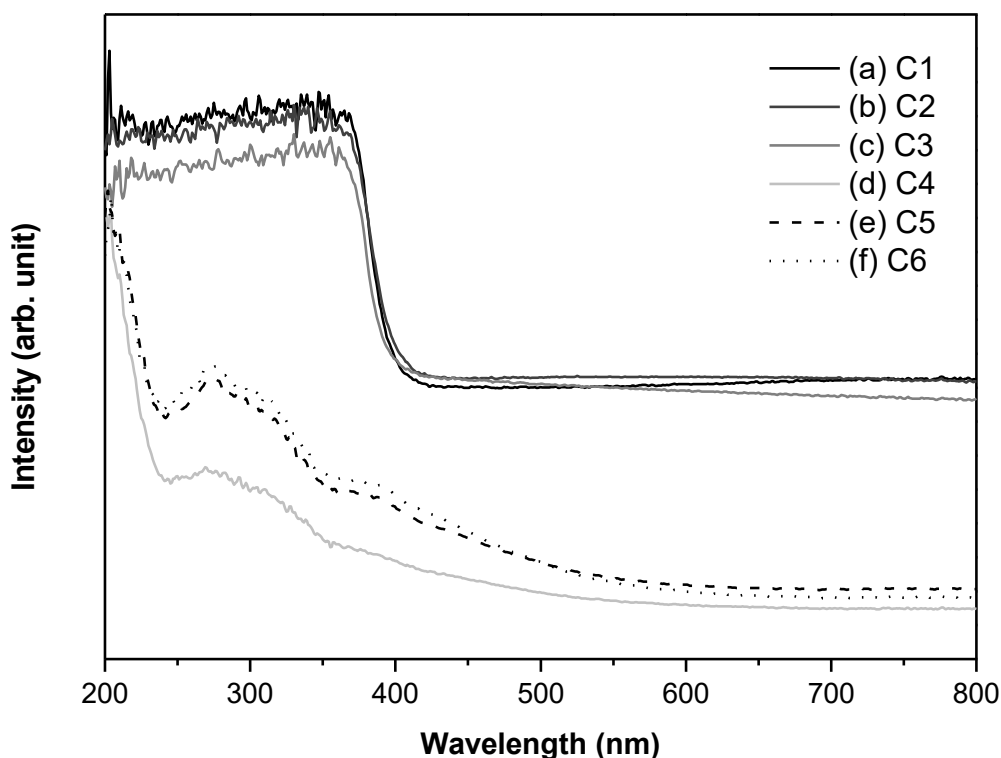


Fig. 7. UV-Vis spectra of chitosan-modified ZnO nanoparticles.

nanoparticles with chitosan tend to agglomerate into bulky aggregates. When the crystallite size is reduced to 21.1-28.2 nm in samples C4-C6, microscale aggregates are also observed but the surface area is clearly increased by smaller agglomeration and the inclusion of pores.

Antifungal Properties

In Fig. 4, photographs of pieces of tube sedge basketry without coating (the control) and conventional lacquer coating indicate the onset of fungi growth after 10 days. For 20 days, fungi have grown and substantially covered the surface. By coating with chitosan-modified ZnO, *Aspergillus* sp. still increasingly grows from 1 to 20 days with an exception of sample C5. The fungi inhibition by this chitosan-modified ZnO is attributed to the stress response in fungal hyphae and generation of hydrogen peroxide [5-10]. The antifungal activity in this sample can be related to the lowest crystallite size of ZnO encapsulated by chitosan. The smaller crystallite and agglomeration promote the fungicide by virtue of the increased surface-to-volume ratio. Only one fungal strain is tested in this work but antifungal activities of ZnO have been previously demonstrated on

others. In addition to *Aspergillus* sp., there are reports on the inhibitions of *Botrytis cinerea* [5], *Penicillium expansum* [5], *Trichoderma harzianum* [9], *Fusarium* sp.[10], *Rhizopus stolonifer* [9, 20], *Candida albicans* [20], *A. flavus* [9], *A. nidulans* [9], *A. brasiliensis* [21], *A. niger* [22] and *T. reesei* [22].

UV-Vis absorption

Fig. 5 compares UV-Vis absorption spectra of ZnO with varying chitosan in the synthesis. Again, absorption characteristics are divided into 2 groups. For samples C1-C3, the absorption is pronounced in the entire UV range of 200-400 nm without any distinct peak. The absorbance then drops to minimum in the visible regime. The spectra, resembling those of ZnO with a different morphology in the previous reports [23], indicate the potential use as sun-screens coating. By contrast, samples C4-C6 with low amounts of chitosan do not have a flat response in the UV range. The UV absorbance is lower and exhibit a peak around 270 nm. The peak is related to the size of ZnO nanoparticles and the capping agents adsorbed at the surface of ZnO inhibit the growth of ZnO nanostructures in certain directions [14]. The different UV-Vis absorption characteristics

in samples C1-C3 is due to the crystallite size regulated by chitosan [3, 8, 12, 13] and the agglomeration into microscale aggregates which could also affect photocatalytic properties [24].

CONCLUSIONS

ZnO nanoparticles were synthesized from the reaction between $\text{Zn}(\text{CH}_3\text{COO})_2 \cdot 2\text{H}_2\text{O}$ and NaOH. Chitosan of varying amounts was added to regulate the crystallite size of ZnO. Large UV absorbance in an extended wavelength range was obtained when large ZnO crystallites agglomerate into bulky aggregates due to an excessive amount of chitosan. On the other hand, the inhibition of *Aspergillus* sp. on tube sedge basketry was more effective in the case of smaller ZnO crystallite size and higher surface-to-volume ratio. It follows that chitosan-modified ZnO can be implemented in sun-screen and antifungal coating on local handicrafts.

ACKNOWLEDGEMENTS

This work is funded by SciUS-TSU and NECTEC-NSTR. The authors would like to thank Scientific Equipment Center of Prince of Songkla University and Thaksin University for the access to characterization facilities.

CONFLICT OF INTEREST

The authors declare that there are no conflicts of interest regarding this article.

REFERENCE

- Anitha R, Ramesh K V, Ravishankar T N, Sudheer Kumar K H, Ramakrishna T. Cytotoxicity, Antibacterial and Antifungal Activities of ZnO Nanoparticles Prepared by the *Artocarpus Gomezianus* Fruit Mediated Facile Green Combustion Method. *J Sci: Adv Mater Div*, 2018;3:440-451.
- Lalithambika K C, Thayumanavan A, Ravichandran K, Sriram S. Photocatalytic and Antibacterial Activities of Eco-Friendly Green Synthesized ZnO And NiO Nanoparticles. *J Mater Sci: Mater Electron*, 2017;28:2062-2068.
- Mohammadi-Aloucheh R, Habibi-Yangjeh A, Bayrami A, Latifi-Navid S, Asadi A. Green Synthesis of ZnO and ZnO/CuO Nanocomposites in *Mentha Longifolia* Leaf Extract: Characterization and their Application as Antibacterial Agents. *J Mater Sci: Mater Electron*, 2018;29:13596-13605.
- Alaghemand A, Khaghani S, Bihanta M R, Gomarlan M, Ghorbanpour M. Green Synthesis of Zinc Oxide Nanoparticles Using *Nigella Sativa* L. Extract: The Effect on the Height and Number of Branches. *J Nanostruct*, 2018;8(1):82-88.
- He L, Liu Y, Mustapha A, Lin M. Antifungal Activity of Zinc Oxide Nanoparticles Against *Botrytis Cinerea* and *Penicillium Expansum*. *Microbiol Res*, 2011;166:207-215.
- Prasad V, Shaikh A J, Kathe A A, Bisoyi D K, Verma A K. Functional Behaviour of Paper Coated with Zinc Oxide-Soluble Starch Nanocomposites. *J Mater Process Technol*, 2010;210:1962-1967.
- Anupama C, Kaphe A, Udayabhanu, Nagaraju G. Aegle Marmelos Assisted Facile Combustion Synthesis of Multifunctional ZnO Nanoparticles: Study of their Photoluminescence, Photocatalytic and Antimicrobial Activities. *J Mater Sci: Mater Electron*, 2018;29:4238-4249.
- Jamdagni P, Rana J S, Khatri P, Nehra K. Comparative Account of Antifungal Activity of Green and Chemically Synthesized Zinc Oxide Nanoparticles in Combination with Agricultural Fungicides. *Int J Nano Dimens*, 2018;9:198-208.
- Gunalan S, Sivaraja R, Rajendran V. Green Synthesized ZnO Nanoparticles Against Bacterial and Fungal Pathogens. *Prog Nat Sci: Mater Int*, 2012;22:693-700.
- Sharma D, Rajput J, Kaith B S, Kaur M, Sharma S. Synthesis of ZnO Nanoparticles and Study of their Antibacterial and Antifungal Properties. *Thin Solid Films*, 2010;519:1224-1229.
- Jongprateep O, Meesombad K, Techapiesanchaorenkij R, Surawathanawises K, Siwayaprahm P, Watthanarat P. Influences of Chemical Composition, Microstructure and Bandgap Energy on Photocatalytic and Antimicrobial Activities of ZnO and Ag-Doped ZnO by Solution Combustion Technique. *J Met Mater Miner*, 2019;29:78-85.
- Ravichandran K, Uma R, Sakthivel B, Gobalakrishnan S, Praseetha P K. Influence of Co + F Doping on the Physical and Antibacterial Properties of ZnO Nanopowders Prepared by a Simple Soft Chemical Method. *J Mater Sci: Mater Electron*, 2016;27:1609-615.
- Rana S B, Singh R P P. Investigation of Structural, Optical, Magnetic Properties and Antibacterial Activity of Ni-Doped Zinc Oxide Nanoparticles. *J Mater Sci: Mater Electron*, 2016;27:9346-9355.
- Anandan M, Dinesh S, Krishnakumar N, Balamurugan K. Improved Photocatalytic Properties and Anti-Bacterial Activity of Size Reduced ZnO Nanoparticles via PEG-Assisted Precipitation Route. *J Mater Sci: Mater Electron*, 2016;27:12517-12526.
- Nithya A, Jothivenkatachalam K. Chitosan Assisted Synthesis of ZnO Nanoparticles: An Efficient Solar Light Driven Photocatalyst and Evaluation of Antibacterial Activity. *J Mater Sci: Mater Electron*, 2015;26:10207-10216.
- Mirmohseni A, Azizi M, Dorraji M S S. A Promising Ternary Nanohybrid of Copper@Zinc Oxide Intercalated with Polyaniline for Simultaneous Antistatic and Antibacterial Applications. *J Coat Technol Res*, 2019;16:1411-1422.
- Bomila R, Suresh S, Srinivasan S. Synthesis, Characterization and Comparative Studies of Dual Doped ZnO Nanoparticles for Photocatalytic Applications. *J Mater Sci: Mater Electron*, 2019;30:582-592.
- Rajesh S, Yadav L S R, Thyagarajan K. Structural, Optical, Thermal and Photocatalytic Properties of ZnO Nanoparticles of Betel Leave by Using Green Synthesis Method. *J Nanostruct* 2016;6(3):250-255.
- Maensiri S, Laokul P, Promarak V. Synthesis and Optical Properties of Nanocrystalline ZnO Powders by a Simple Method Using Zinc Acetate Dihydrate and Poly(Vinyl Pyrrolidone). *J Cryst Growth*, 2006;289:102-106.
- Sawai J, Yoshikawa T. Quantitative Evaluation of Antifungal Activity of Metallic Oxide Powders (MgO, CaO and ZnO) by an Indirect Conductimetric Assay. *J Appl Microbiol*, 2004;96:803-809.
- Vlad S, Tanase C, Macocinschi D, Ciobanu C, Balaes T, Filip D, Gostin I N, Gradinaru L M. Antifungal Behaviour of Polyurethane Membranes with Zinc Oxide Nanoparticles. *Dig J Nanomater Biostruct*, 2012;7:51-58.
- El-Feky O. M, Hassan E A, Fadel S M, Hassan M L. Use of ZnO Nanoparticles for Protecting Oil Paintings on Paper Support

- Against Dirt, Fungal Attack, and UV Aging. *J Cult Herit*, 2014;15:165-172.
23. Pholnak C, Latte N, Sirisathikul C, Lertworapreecha M, Suwanboon S. Antifungal Mulberry Papers Modified with Microclusters of Pyramidal Zinc Oxide. *Cellulose Chem Technol*, 2018;52:689-694.
24. Hakimi B, Ghorbanpour M, Feizi A. A Comparative Study of Photocatalytic Activity of ZnO/ Activated Carbon Nanocomposites Prepared by Solid-state and Conventional Precipitation Methods. *J Nanostruct*, 2018; 8(3):259-265.